Anisotropic Interaction of Halogen Atom in C_2H_5X (X = Cl, F) with He*(2^3S) As Probed by Two-Dimensional Penning Ionization Electron Spectroscopy

Kohei Imura, Naoki Kishimoto, and Koichi Ohno*

Department of Chemistry, Graduate School of Science, Tohoku University, Aramaki, Aoba-ku, Sendai 980-8578, Japan

Received: October 31, 2000; In Final Form: April 16, 2001

Penning ionization of C_2H_5X (X = Cl, F) upon collision with metastable He*(2^3S) atoms was studied by two-dimensional (collision-energy/electron energy resolved) Penning ionization electron spectroscopy. Partial ionization cross sections are found to be larger for ionization from orbitals having n_x characters. Collision energy dependence of the partial cross sections, which reflects interaction potential energy between the molecule and He(2^3S), indicates anisotropic interaction potentials around the molecule. As elucidate with the aid of calculated energy surfaces for the chemically related systems Li−C_2H_5X (X = Cl, F), a different trend was found in the interaction around C−X axis: for the former the attractive interaction was dominated around the perpendicular directions to the C−Cl bond axis, while for the C−F bond the attractive interaction was localized around the collinear axis.

I. Introduction

It is well-known that the shape and the spread of molecular orbital play the central role in the chemical reactions. Penning ionization electron spectroscopy is one of the most suitable methods for probing electron distributions of molecular orbitals (MOs).[1,2] Penning ionization[3] can occur when a molecule M collides with a metastable atom A* ($A^* + M \rightarrow A + M^+ + e^-$).

The Penning ionization process can be explained by the electron exchange model proposed by Hotop and Niehaus.[4] On the basis of this model, overlap of orbitals related to the electron exchange is required. Ohno et al.[1,5] successfully applied the exterior electron density (EED) model to this process in order to account for experimental branching ratios for Penning ionization. Larger electron distribution outside the van der Waals radii brings larger overlap of mutual orbitals involving electron exchange with resultant large ionization probability. The reaction probability depends on both the electron distribution of the MO and the interaction of the reagents. The kinetic energy of the ejected electron depends on the energy difference between the entrance potential energy surface of A* + M and the exit potential energy surface of $A + M^+$ at the ionization point.[6] Thus the Penning ionization electron spectrum (PIES) does not give the ionization potential (IP) of the isolated molecule, which can be determined by He I ultraviolet photoelectron spectroscopy. Then there are systematic kinetic energy shifts between PIES and ultraviolet photoelectron spectrum (UPS), corresponding to the energy difference between the metastable atom and the photon energy. The information on the interaction potential of the entrance channel can be obtained from the peak energy shift if the exit potential can be assumed as flat in the ionization region. In the case of a positive peak energy shift, the interaction is repulsive, and a negative shift can be ascribed to an attractive interaction.

The branching ratio for the population of the different electronic bands in PIES corresponds to the partial ionization cross sections. In many cases, attractive interactions enhance the ionization cross section, while there are some exceptions such as the n_O orbital in the carbonyl group.[7] The ionization cross section depends not only on the electron distribution of the MO and characteristic of the interaction but also on the collision energy of the metastable atom. Therefore, the observation of collision-energy-dependent cross sections provides valuable information about the interaction, especially when the peak energy shift cannot be determined. Two-dimensional PIES (2D-PIES) has been recently developed in our laboratory,[8] in which ionization cross sections are determined as functions of both electron kinetic energy (E_e) and metastable atom collision energy (E_c). This technique makes it possible to study the collision-energy dependence of the partial ionization cross sections (CEDPICS) and collision-energy-resolved PIES (CERPIES), and thus the state-resolved measurement of partial cross sections for the *i*th ionic state enables us to investigate the anisotropic potential surface around the target molecule.

Anisotropic interactions around Cl atoms in *trans*-, *cis*-, and *iso*-dichloroethylenes,[9] vinyl chloride,[10,11] $(CH_3)CCl$,[12] and CH_3-Cl[13] with He*(2^3S) atom have been reported. Although attractive interactions were found around the Cl atom, suggesting that perpendicular approach of the He*(2^3S) atom with respect to C−Cl bond axis is more attractive, further discussions are necessary for a detailed understanding of the anisotropic interaction around the halogen atom. Recently, Alberti et al. studied anisotropy effects in CH_3Cl ionization by metastable neon atoms.[14] They constituted the real part of the potential energy surface semiempirically and reported that the strongest attractive interaction was located around the angle of 45° with respect to the C−Cl bond axis. Very recently, Yamato et al.[15] have studied Penning ionization of $CHCl_3$ by Ar*($^3P_{0,2}$), using a combination of a time-of-flight technique and an electric hexapole orientation technique, and discussed the correlation between collision energy and steric effects. Anisotropy in chemical reactions by using aligned molecules have been reported.[16,17] On the other hand, reaction anisotropy around the F atom in the Penning ionization has never been reported so

* Author to whom correspondence should be addressed.

10.1021/jp004036p CCC: $20.00
Published on Web 06/07/2001

far, while in the reaction of Sr, K, and Li with HF, Loesch and co-workers have reported the effect of the HF alignment on the reactivity.[17,18]

From a chemical point of view, it is very interesting and important to reveal the interaction feature of atoms, which have the same number of valence electrons, because it is well-known that atoms having the same number of valence electrons such as halogen atoms show similar and systematic characteristics in many reaction systems from a macroscopic point of view. One question can be raised from a microscopic point of view whether the reaction dynamics of these species are similar or not. The anisotropic interaction around urea and thiourea ($(NH_2)_2C{=}X$, X = O, S) was studied, and a different trend was reported in the interaction around the C═X (X = O, S) group; an attractive interaction was found for the perpendicular direction around the C═S axis where the 3p orbital of the S atom extends, while the collinear direction along the C═O bond was found to be most attractive.[19] This result suggested that even the atoms with the same number of valence electrons behave in quite a different way.

In this paper, we studied the interaction anisotropy around Cl or F atom. We have measured 2D-PIES of C_2H_5X (X = Cl, or F) in order to get further insight about the anisotropic interaction around these halogen atoms and to obtain systematic understanding for reaction dynamics of the atoms that possess same number of valence electrons. Furthermore, the validity of the semiempirical electrostatic model adopted by Alberti et al.[14] for simulating collision-energy-dependent ionization cross sections will be discussed.

II. Experimental Section

High purity samples (C_2H_5Cl and C_2H_5F) were commercially purchased and used without further purification. The experimental apparatus for He*(2^3S) Penning ionization electron spectroscopy has been reported previously.[12,20−22] Therefore only a brief description will be given below. The metastable He* beam was generated by a discharge nozzle source with a tantalum hollow cathode. The metastable He* atoms in the 2^1S metastable state are removed by a helium discharge (quench) lamp after passing through the skimmer. Ionic and Rydberg species produced by the discharge were removed by an electric deflector. The He(2^3S) metastable beam enters into the collision cell where sample gas was introduced. Electrons produced by Penning ionization were measured by a hemispherical electrostatic deflection type analyzer using an electron collection angle 90° relative to the incident He* beam. He I UPS were measured by using He I resonance photons (584 nm, 21.22 eV) produced by a dc-discharge in pure helium gas. The kinetic energy of the ejected electrons was measured by the analyzer using an electron collection angle of 90° relative to the incident photon beam. The energy resolution of the electron energy analyzer was estimated to be 70 meV from the full width at half-maximum (fwhm) of the $Ar^+(^2P_{3/2})$ peak in the He I UPS of Ar atoms. The transmission efficiency curve of the electron analyzer was determined by comparing our UPS data of several molecules with those by Gardner and Samson[23] and Kimura et al.[24] Calibration of the electron energy scale was made by reference to the lowest ionic state of N_2 mixed with the sample molecule in He I UPS (E_e = 5.639 eV)[25] and He* (2^3S) PIES (E_e = 4.292 eV).[26,27]

In the collision-energy-resolved experiments, 2D-PIES, the metastable atom beam was modulated by a pseudo-random chopper,[28] rotating at about 400 Hz, and introduced into the reaction cell; the latter was located 504 mm downstream from the chopper disk, and the sample pressure was kept constant. The resolution of the electron analyzer was lowered to 250 meV in order to gain higher electron counting rates. Time-dependent electron signals for each kinetic electron energy (E_e) were recorded while scanning the electron energy in 35 meV steps. The 2D Penning ionization data as functions of both E_e and t were stored in a memory of a computer. The velocity dependence of the electron signals was obtained from the time dependent signals by Hadamard transformation in which the time-dependent signals were cross-correlated with the complementary slit sequence of the pseudo-random chopper. Similarly, the velocity distribution of the metastable He*(2^3S) beam was determined by measuring the intensity of secondary electrons emitted from an inserted stainless plate. The 2D Penning ionization cross section $\sigma(E_e, v_r)$ was obtained via normalization to the velocity distribution $I_{He^*}(v_{He^*})$ of the He*(2^3S) atoms.

$$\sigma(E_e, v_r) = c[I_e(E_e, v_{He^*})/I_{He^*}(v_{He^*})](v_{He^*}/v_r) \quad (1)$$

$$v_r = [v_{He^*}^2 + 3kT/M]^{1/2} \quad (2)$$

where c is a proportionality constant, v_r the relative velocity of metastable atoms averaged over the velocity of the sample molecule, k the Boltzmann constants, T the gas temperature (300 K), and M the mass of the sample molecule, respectively. Finally, $\sigma(E_e, v_r)$ is converted to $\sigma(E_e, E_c)$ as functions of E_e and E_c by the following relation:

$$E_c = \mu v_r^2/2 \quad (3)$$

where μ is the reduced mass of the reaction system.

III. Calculations

We performed ab initio Hartree−Fock self-consistent field (SCF) calculations with 4-31G basis functions for neutral sample molecules in order to obtain electron density contour maps and schematic diagrams of MOs. The geometries of the molecules were taken from microwave spectroscopic studies.[29−31] In the electron density maps, thick solid curves indicate the repulsive molecular surface approximated by van der Waals radii[32] (r_C = 1.7 Å, r_H = 1.2 Å, r_{Cl} = 1.8 Å, r_F = 1.35 Å). In schematic diagrams of MOs, circles and ellipses were used. Solid circles show valence s orbitals, where couples of ellipses and dashed circles show in-plane and out-of-plane components of p orbitals, respectively.

Interaction potential energies between He(2^3S) and M in various directions and angles were also calculated on the basis of the well-known resemblance between He(2^3S) and Li(2^2S);[33] the shape of the velocity dependence of the total scattering cross section of He(2^3S) by He, Ar, and Kr is very similar to that of Li, and the location of the interaction potential well and its depth are similar for He*(2^3S) and Li with various targets.[34−37] Recently, a precise estimate of the similarity[38] has been made for atomic targets; the well depths for the Li + Y (Y = H, Li, Na, K, Hg) systems were found to be 10% to 20% larger than those for He*(2^3S) + Y. Although for molecular targets M, a direct comparison between the interactions of Li + M and He* (2^3S) + M has never been reported so far, the observed peak energy shifts between PIES and UPS, which was relevant to the interaction potentials between the reagents, were well reproduced by the Li + M potentials calculations for numerous compounds.[7−12,19] Because of these findings and the difficulties associated with the calculation of excited states, Li was used in

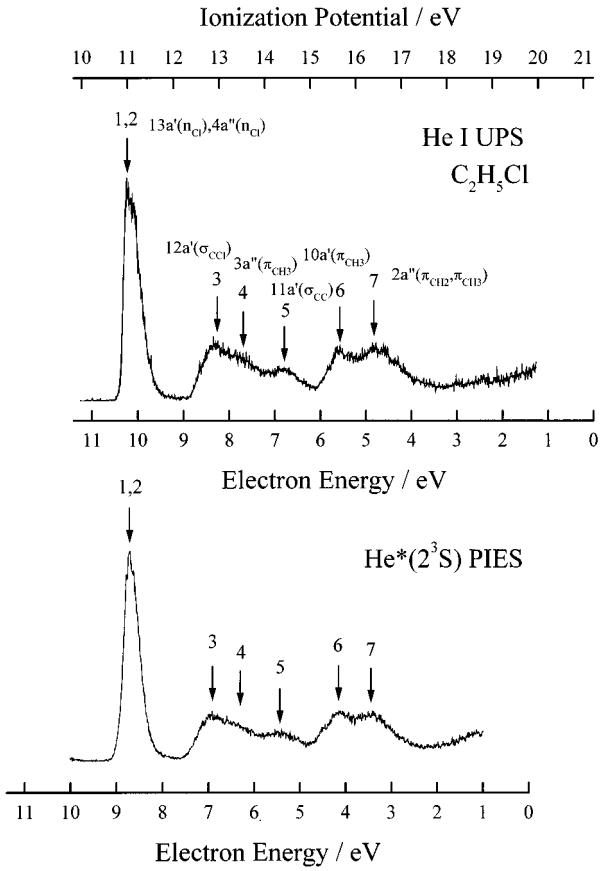

Figure 1. He I UPS and He(2^3S) PIES of C_2H_5Cl.

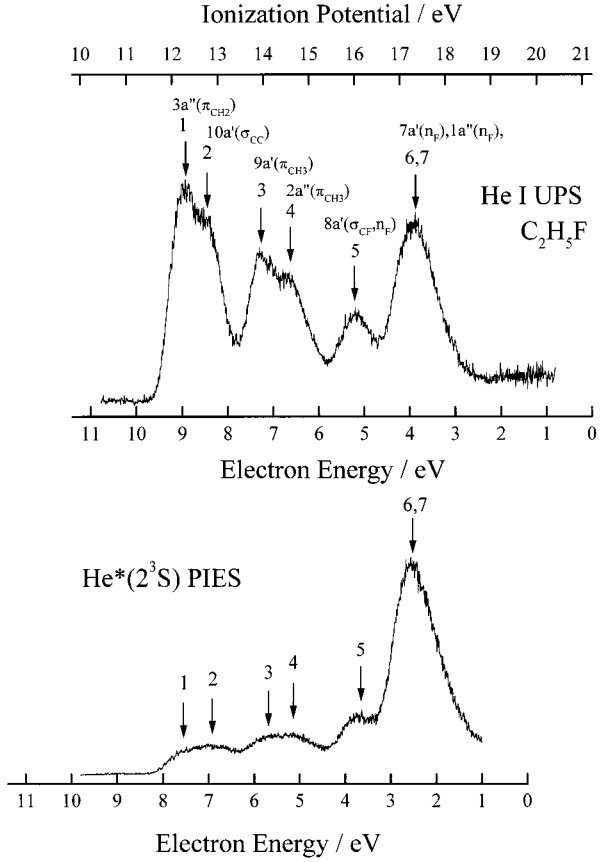

Figure 2. He I UPS and He(2^3S) PIES of C_2H_5F.

this study in place of He*(2^3S). Thus the interaction potential M−Li(2^2S), $V^*(R, \theta)$ (where R and θ are the Li-X distance and ∠CXLi angle), was calculated by moving the Li atom toward halogen atom and keeping the molecular geometries fixed at the experimental values; this assumption meant that the geometry change by the approach of metastable atom was negligible in the collisional ionization process. For calculating the interaction potential, standard 6-311++G** basis set was used, and the correlation energy correction was partially taken into account by using second-order Møller−Plesset perturbation theory (MP2). All the calculations in this study were performed with the GAUSSIAN 94 quantum chemistry program.[39] The ionization potentials for C_2H_5Cl and C_2H_5F were calculated at the experimentally determined geometries using the outer valence Green's function (OVGF) method[40,41] as incorporated in Gaussian 94.

IV. Results

Figures 1 and 2 show the He I UPS and He*(2^3S) PIES of C_2H_5Cl and C_2H_5F, respectively. The electron energy scale for PIES is shifted relative to that of UPS by the excitation energy difference between He I photons (21.22 eV) and He*(2^3S) (19.82 eV), namely 1.40 eV.

Figures 3 and 4 show the collision-energy-resolved PIES (CERPIES) obtained from the 2D spectra of C_2H_5Cl and C_2H_5F. "Hot" spectra at the higher collision energy (ca. 250 meV) are shown by dashed curves, and the "cold" ones at the lower collision energy (ca. 90 meV) are shown by solid curves.

Figures 5 and 6 show the log σ versus log E_c plots of CEDPICS in the collision energy range of 90−300 meV for C_2H_5Cl and C_2H_5F, respectively. The CEDPICS was obtained from the 2D-PIES $\sigma(E_e,E_c)$ within an appropriate range of E_e-

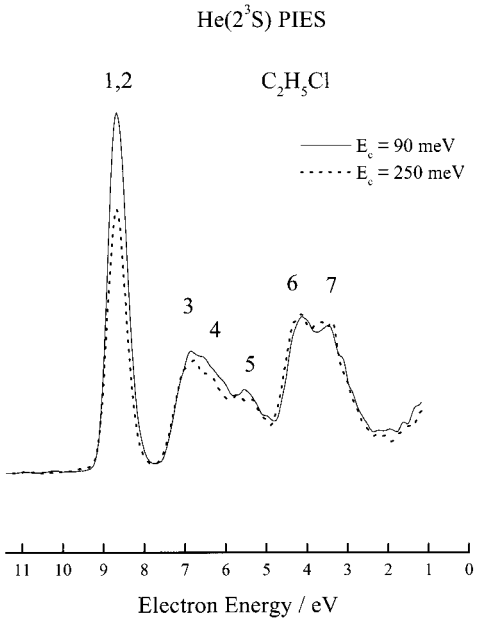

Figure 3. Collision-energy-resolved He(2^3S) PIES of C_2H_5Cl.

(typically electron energy resolution of analyzer, 250 meV) to avoid the contribution from neighboring bands. Electron density maps are also shown in the figures in order to grasp the effective access direction of He*. The calculated electron density maps for σ orbitals are shown on the C−C−X (X = Cl or F) molecular plane, and those for π orbitals are shown on a plane at a height of 1.7 Å (van der Waals radii of C atom) from the molecular plane.

Figures 7 and 8 show the calculated interaction potential energy curves between ground-state Li and C_2H_5Cl and C_2H_5F,

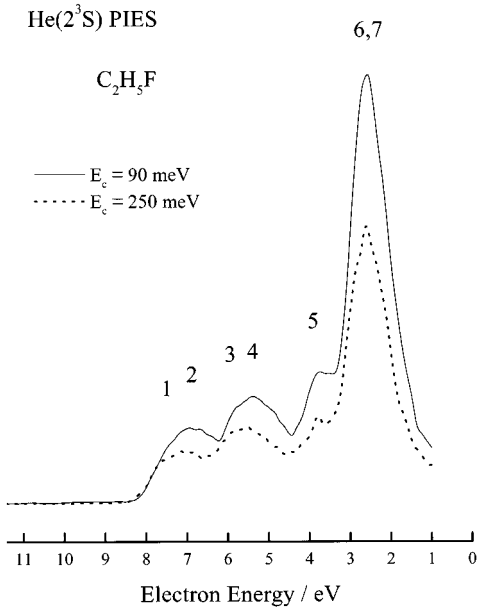

Figure 4. Collision-energy-resolved He(2^3S) PIES of C_2H_5F.

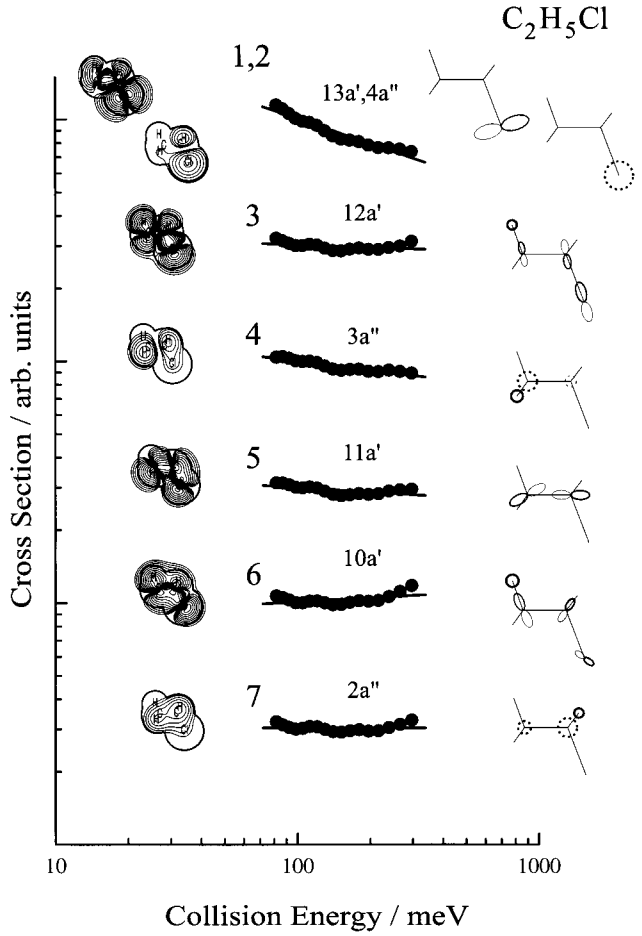

Figure 5. Collision-energy dependence of partial ionization cross sections for C_2H_5Cl collided by He(2^3S) atom. The contour plots show electron density maps for respective MOs.

respectively. The potential energies are shown as functions of Li−X distance and ∠CXLi angle. Calculations are done at the MP2/6-311++G** level of theory. As can be seen in Figure 7, there is a strong anisotropy for the interactions among the perpendicular directions with respect to the C−Cl bond axis. This arises from the effect of repulsive interactions around the

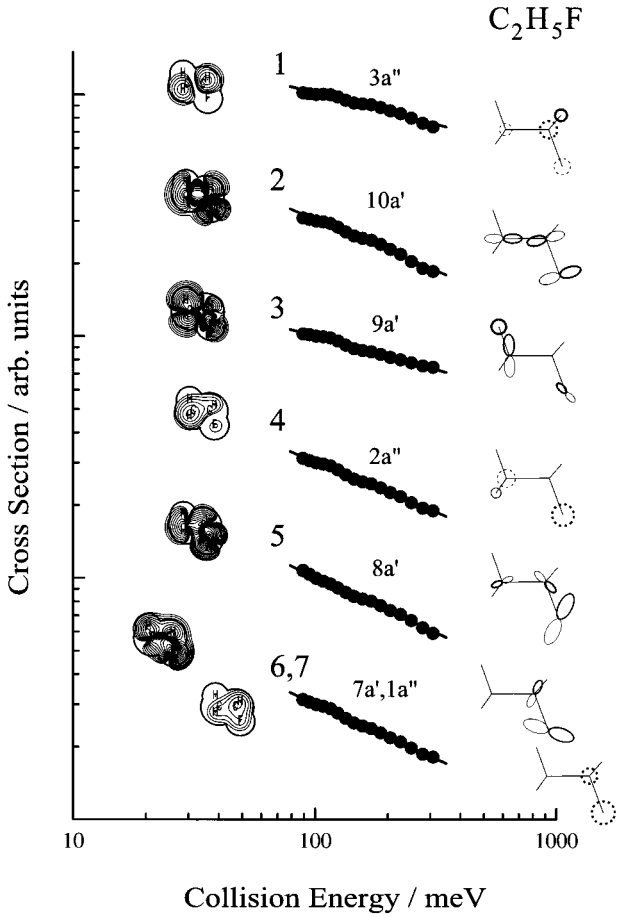

Figure 6. Collision-energy dependence of partial ionization cross sections for C_2H_5F collided by He(2^3S) atom. The contour plots show electron density maps for respective MOs.

CH_3 group for perpendicular approach (▲) coming from the CH_3 group. The same argument is applicable for explaining the stronger repulsive interaction for perpendicular approach coming from the CH_3 group in the case of Li + C_2H_5F system as can be seen in Figure 8. Anisotropy among the perpendicular interactions is more pronounced for C_2H_5F because the van der Waals radius of the F atom is smaller than that of the Cl atom. We have also calculated potential energy curves shown in Figure 9 as a function of ∠CXLi angle ((a) ϕ in the perpendicular plane with respect to C−X axis and (b) θ in the perpendicular plane with respect to molecular plane containing C, C, and X atoms) with fixed distance 2.5 and 2.0 Å for X = Cl and F atom, respectively. These values correspond to the distances of the potential minimum as shown in Figures 7 and 8. The most attractive interactions were again found around the perpendicular direction to the C−Cl axis in Li−C_2H_5Cl and for the nearly collinear direction to the C−F axis in Li−C_2H_5F as shown in Figure 9a,b.

Table 1 summarizes experimentally observed and calculated IPs, experimental peak energy shifts (ΔE), slope parameters of CEDPICS (m), and the assignment of the bands. Slope parameters are obtained from the log σ vs log E_c plots in a collision energy range for 90−300 meV by a least-squares method. Vertical IPs are determined from He I UPS. The peak energy shifts are obtained as the difference between the peak position (E_{PIES}; electron energy scale) and the "nominal" value (E_0 = difference between metastable excitation energy and sample IP): $\Delta E = E_{PIES} - E_0$.

TABLE 1: Band Assignment, UPS Ionization Potentials (IP/eV), Peak Energy Shifts (Δ*E*/meV), and Slope Parameters (*m*) C_2H_5Cl and C_2H_5F

molecule	band	UPS IP_{obsd}/eV	IP_{OVGF}/eV (pole strength)	orbital character	Δ*E*/meV	*m*
C_2H_5Cl	1,2	10.98 ± 0.02	10.87(0.92)	13a′(n_{Cl})	−130 ± 50	−0.34 ± 0.03
		11.07 ± 0.05	10.92(0.92)	4a″(n_{Cl})		
	3	13.01 ± 0.05	13.11(0.92)	12a′(σ_{CCl})	0 ± 100	−0.04 ± 0.05
	4	13.51 ± 0.05	13.46(0.92)	3a″(π_{CH_3})	90 ± 130	−0.12 ± 0.05
	5	14.42 ± 0.05	13.92(0.91)	11a′(σ_{CC})	70 ± 80	−0.06 ± 0.04
	6	15.65 ± 0.03	15.49(0.91)	10a′(π_{CH_3})	50 ± 70	+0.05 ± 0.05
	7	16.39 ± 0.04	16.24(0.91)	2a″(π_{CH_2}, π_{CH_3})	80 ± 80	+0.03 ± 0.04
C_2H_5F	1	12.29 ± 0.02	12.60(0.93)	3a″(π_{CH_2})	50 ± 80	−0.26 ± 0.05
	2	12.79 ± 0.03	12.83(0.92)	10a′(σ_{CC})	−100 ± 130	−0.42 ± 0.04
	3	13.95 ± 0.02	14.25(0.92)	9a′(π_{CH_3})	−170 ± 120	−0.28 ± 0.04
	4	14.58 ± 0.04	14.64(0.92)	2a″(π_{CH_3})	−100 ± 120	−0.42 ± 0.04
	5	16.00± 0.02	15.99(0.91)	8a′(σ_{CF}, n_F)	−160 ± 80	−0.46 ± 0.04
	6,7	17.30 ± 0.05	17.19(0.92)	7a′(n_F)	−140 ± 100	−0.44 ± 0.03
			17.20(0.92)	1a″(n_F)		

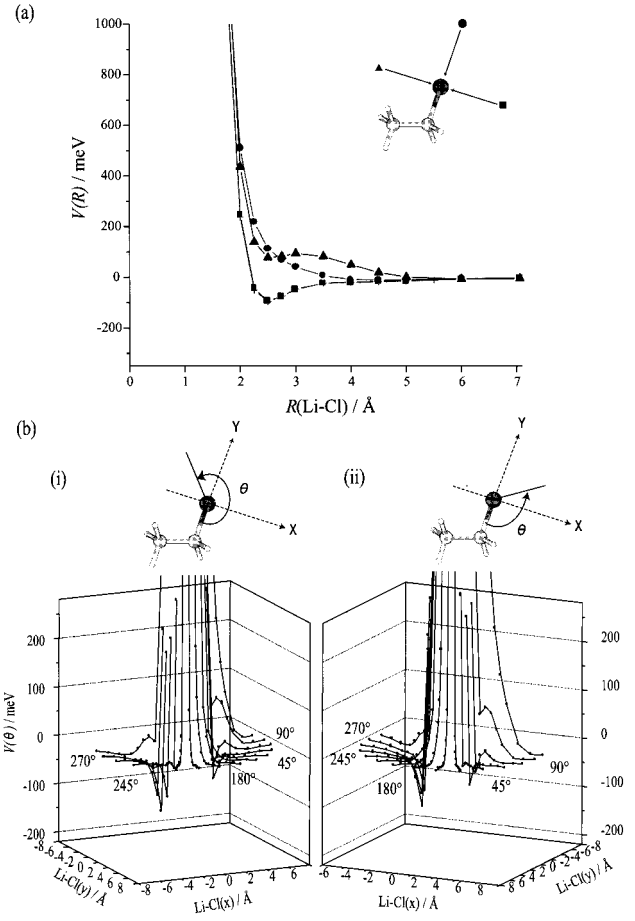

Figure 7. Model potential curves V(*R*) obtained by MP2 calculations for C_2H_5Cl and Li as a function of distance *R*; (a) around the Cl atom for out-of plane direction(+) and in-plane direction with ∠CClLi angle of 90°(■), 180°(●), 270°(▲). (b) The origin of the coordinate is Cl atom. The *x* and *y* axes are defined in the figure. The ∠CClLi angle is indicated for each curve. ((i) larger ∠CClLi angle view. (ii) smaller angle view.)

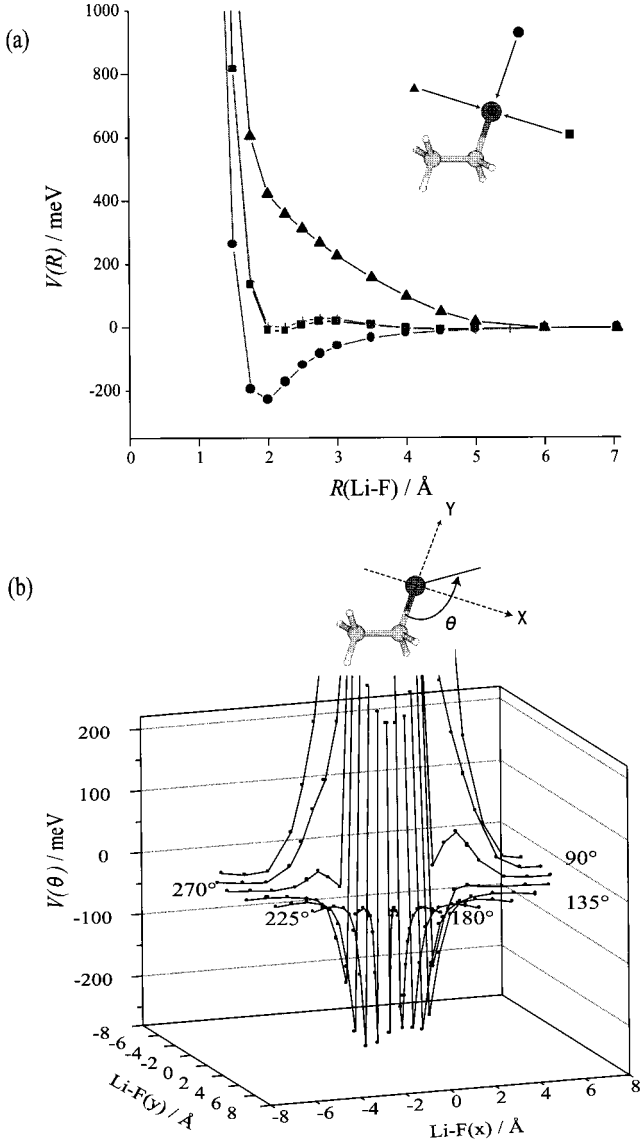

Figure 8. Model potential curves *V*(*R*) obtained by MP2 calculations for C_2H_5F and Li as a function of distance *R*; (a) around the F atom for out-of plane direction(+) and in-plane direction with ∠CFLi angle of 90°(■), 180°(●), 270°(▲). (b) The origin of the coordinate is F atom. *x* and *y* axes are defined in the figure. The ∠CFLi angle is indicated for each curve.

V. Discussion

A. UPS and PIES of C_2H_5Cl. UPS of C_2H_5Cl molecule has been reported previously.[42,43] It is hard to resolve bands 1 and 2 because they lie very close to each other. To make matters worse, the first bands are accompanied by spin−orbit splittings. In the present study, the energy difference of these bands was estimated as about 100 meV by the OVGF calculation. This result indicates that band 1 has 13a′ character, and band 2 possesses 4a″ character while there is no evidence for ascribing the splitting to either origin. It is found that the assignments of bands 3−7 are consistent with those reported by Kimura et al.[24] Furthermore, the observed IPs and the calculated IPs show good

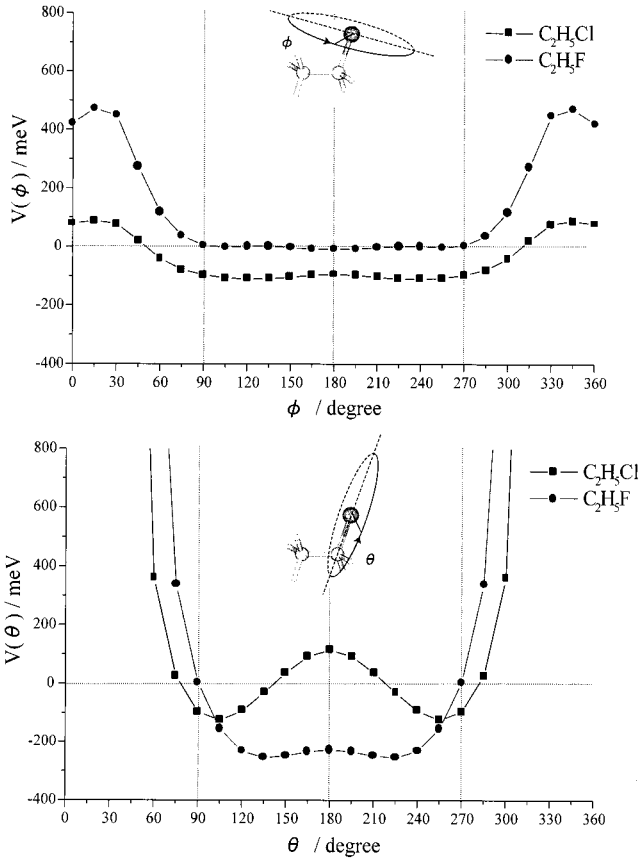

Figure 9. Model potential energy curves obtained by MP2 calculations for C_2H_5X (X = Cl, F) and Li atom as a function of ∠CXLi angle (a)ϕ in the plane perpendicular to the C−X axis and (b) θ to the molecular plane defined by the C, C, and X atoms. Distance between X (X = Cl, F) and Li atoms is fixed at 3.0 and 2.5 Å, respectively.

agreement within 0.5 eV as in the earlier work by the OVGF calculations.[11,19,41,44] The pole strengths of all calculated bands are over 0.9 indicating that ionization occurs from the corresponding molecular orbital.

PIES of C_2H_5Cl was also studied previously,[45] and it was reported that the relative band intensities varied with respect to UPS band intensities. In the present study, peak energy shifts of these bands were obtained in addition. Bands 1, 2 are very much enhanced with respect to the other bands 3−7 which are due to bonding orbitals having their electron distributions mostly on the ethyl group. The electron density map shown at the right side of Figure 5 indicates that n_{Cl} orbitals are exposed to the outside beyond the repulsive potential surface illustrated by solid curves. Therefore, the strong intensities for the n_{Cl} bands were explained by the large exterior electron distribution of the n_{Cl} orbitals. The peak energy shift for each band with respect to UPS is summarized in Table 1. Only bands 1 and 2 give negative shifts, while the other bands yield positive shifts. If the interaction potential of He* and the molecule is repulsive, the peak energy shift is likely to be positive since the outgoing potential energy surface near the ionization region can be assumed to be nearly flat as a reasonable approximation. The opposite negative shift case, which shows an attractive interaction in accord with the case of $C_2H_2Cl_2$,[9] is found for bands 1, 2 (n_{Cl} orbital). It is noted that this fact is also found in the calculated results, see Figures 7 and 9. Namely, the p-lobe of the Cl atom perpendicular to the C−Cl band axis, located on the opposite side of the CH_3 group, shows an attractive interaction. It should be noted that the amount of energy shift is almost consistent with the calculated well depth (∼100 meV) of the Li−C_2H_5Cl model system. This fact further supports the validity of the above approximation. It is also noted that the peak shift of band 3 (σ_{CCl}) indicates that the collinear approach of the He* to C−Cl bond axis is not influenced by any strong attractive interaction. This observation also agrees with the results of theoretical calculation, which indicates a repulsive interaction.

B. CEDPICS of C_2H_5Cl Molecule. The slope parameter *m* of the bands 1, 2 in Table 1 has a very large negative value, which indicates a decrease of the ionization cross section with increase of collision energy. When a slower He* metastable atom can approach the reactive region effectively by attractive force, ionization cross section is enhanced for the lower collision energies. Negative slope parameters of these bands are compatible with the negative peak energy shifts. Similar positive slope parameters were observed for bands 6 and 7 since these bands have identical MO character, π_{CH_3}, or π_{CH_2}. This results from a larger exterior electron distribution having a repulsive character outside the van der Waals radii of this molecular orbital. As discussed in the previous work,[21] the slope parameter *m* for log σ vs log E_c plot can be related to parameters *b* and *d* (the definitions are given below) by the equation

$$m = (b/d) - 1/2 \tag{4}$$

Approximating the relation in the simple theoretical model for the ionization cross section σ[34]

$$\sigma(E_c) \propto [\ln(B/E_c)]^2 (E_c/B)^{(b/d)-1/2} \tag{5}$$

where *d* is the effective decay parameter for the interaction potential ($V(R) = B \exp(-dR)$; *R* is the distance) and *b* is the effective decay parameter of the transition probability ($W(R) = C \exp(-bR)$). The parameter *b* can be estimated from the asymptotic decay of the target wave function which is directly related to the lowest IP of the molecule ($b = 2(2IP)^{1/2}$).[46,47,48,49] When the potential energy surface for the entrance channel shows a soft repulsive curve, *m* (= (*b*/*d*)-1/2) value is thought to be large because of the small *d* value and common *b* value for a given molecule. The observed positive slopes of bands 6 and 7 of C_2H_5Cl are consistent with a soft repulsive potential energy curve for the He* atom approach toward the CH_3 group. The slope parameters of bands 3 and 5 are almost the same, but the peak energy shift of band 5 is larger than the one for band 3. This is due to the fact that σ_{CCl} is more active than σ_{CC}, which is consistent with the empirical rule for PIES.[1,45]

C. UPS and PIES of C_2H_5F. The UPS of C_2H_5F has been measured by Kimura and co-workers.[50] IPs obtained in the present study agreed with those reported by Reference 50 within 80 meV. Bands 6 and 7 cannot be resolved due to the small energy difference. OVGF calculation estimated this difference as 10 meV in accord with experimental observation. Calculated pole strength of each band is sufficiently high (>0.9).

PIES of C_2H_5F with He*(2^3S) has not been reported so far. Although separation of each band is not fairly good, we obtained peak energy shifts compared to UPS. Peak energy shift of each band except band 1 shows negative shift. This results from the wide range of strong attractive regions near the F atom, which expands from ca. 90° to ca. 250° of C−F−Li angle as shown in Figures 8(b) and 9(b). This is in clear contrast to the case of the Cl atom, which has attractive region in specific narrower angle with respect to C−Cl bond axis as can be seen in Figures 7(b) and 9(b). Relative peak intensities of bands 5 and 6, 7 become intense compared to the other bands. This can be explained by the EED model as mentioned in the introductory

section, that is, the electron distribution outside the van der Waals radii governs the reactivity of the molecule. It is true that the electron density outside the repulsive surface around the F atom is large, and also this region show the large attractive interaction with the He* atom. As a consequence, metastable atom trajectories, which have a broader range of impact parameters, toward the C_2H_5F molecules are influenced by the attractive force, thus enhancing the reactive cross section. The very strong intensity of band 6,7 is due to the fact that the orbital phase between the F atom and the neighboring atoms matches well and gives larger electron density around the attractive F atom. It is noted that the measured peak energy shift is larger than that of C_2H_5Cl at each band. Moreover, it is valuable to compare the measured peak energy shift with the one obtained in the calculation. The observed peak energy shift can be roughly related to the value of the interaction potential, provided that the exit potential energy surface of $He + M^+$ is nearly flat or slightly attractive at the ionization point. It is found that the observed negative shifts are small compared to one obtained in the calculation. These differences may, however, not be ascribed to an overestimation of the present MP2 calculation. Alternative calculations with B3LYP/6-311+G* yielded a well depth for collinear approach of the Li atom to the C−F molecular axis of 268 meV, that is larger than 228 meV at the MP2 level. (Even smaller basis set gives larger well depth.) The disagreement between the observation and the calculation can be explained as follows. In bands 3 and 4, the orbital characters are π_{CH_3}, and as discussed for C_2H_5Cl, this orbital gives a positive peak shift. Furthermore, the very large electron density distribution outside the van der Waals surface near the opposite side of the F atom is present as shown in Figure 6. It is important to realize that the molecule is not oriented in the present experiment (actually, it is very hard to orient asymmetric top molecule like C_2H_5F), so that collision can take place at any He* incident approach angle with respect to C_2H_5F molecule, since the molecules are randomly oriented. Therefore, the observed peak energy shift reflects contributions from the orbital features at various molecular orientations. Considering these facts mentioned above, relatively small peak energy shifts are understandable for these bands. With regard to band 2, which is related to the larger orbital distribution near the F atom, it is thought that the peak energy shift is not as high as predicted theoretically, because most of the collisions take place at perpendicular directions to the C−F bond axis that has basically repulsive character. Relatively larger negative shift of band 5 can be ascribed to the more strongly attractive electron distribution around the F atom.

D. CEDPICS of C_2H_5F. The slope parameters for all bands show negative values. In particular, it seems that the large values of bands 2, 4, 5, and 6,7 reflect the strong attractive force around F atom. This is one of the evidences that the obtained slope parameters of these bands are nearly coincident. Small values of bands 1 and 3 could arise from the larger repulsive orbital contribution around the CH_3 group. In contrast to C_2H_5Cl, the larger attractive region near F atom plays a central role for He*-(2^3S) Penning ionization, then the strong attractive force becomes a major component besides the repulsive interaction around the CH_3 group. The repulsive interaction around the CH_3 group was clearly observed in the He(2^3S) + C_2H_5Cl system. It is important to realize that as the interaction potential has a large and deep potential well, the reactivity of the molecule drastically is affected by this potential well. Even in the incident He* atoms directly approaching toward the repulsive region, some of the He* trajectories can be influenced by the strong attractive interaction and give reactive trajectories. As a consequence, negative slope parameters for all bands were observed. In other words, strong attractive interactions distributed over a large region can overcome a weak repulsive one. It is noted that the potential depth of Li−C_2H_5F is larger than the collision energy in the present study, while the depth of Li−C_2H_5Cl is smaller.

E. Evaluation of the Potential Energy Surface. The potential energy surface calculated by the ab initio MO method indicates that the potential is very sensitive to the positions of the atoms in interacting species as can be seen in Figures 7, 8, and 9. The most attractive interaction was found around the perpendicular direction to the C−Cl bond axis and around the collinear direction with respect to the C−F bond axis in the C_2H_5X (X = Cl, F), respectively. Actually, it is found that the angle of the Li atom for the most attractive interaction is slightly displaced either from the perpendicular or collinear direction with respect to C−X axis because of the effect of adjacent atoms in the molecule. As can be seen in Figure 7a, the Li atom approaches directed perpendicular to the C−Cl axis (▲,■) show a remarkably different behavior. This difference and general feature of the interaction potential were also well reproduced by B3LYP/6-311+G* calculations.

It seems that to construct the interaction potential empirically is a challenging task even in the relatively small reaction system because the potential energy surface is highly anisotropic because of sensitivity to many features of the reaction system, for instance, bond and atom character, atom position, and so on. Recently, two types of semiempirical interaction potentials of Ne*−CH_3Cl system have been reported.[14,51] In the former paper, the potential energy surface was determined by assuming two main contributions: a weak van der Waals (vdW) component and a "charge transfer" (CT) interaction. This potential showed a weak attractive interaction in the direction perpendicular to the C−Cl axis and a more attractive interaction for collinear approaches toward methyl and Cl atom along the C−Cl axis. In the latter paper, the potential energy surface was refined in order to explain their results of collision-energy-dependent ionization cross sections by taking an electrostatic contribution into account, which comes from the interaction between the permanent C−Cl dipole and a partial positive charge on Ne* produced by a transfer of its excited electron into a sp hybrid orbital. The newly introduced term represents an ion−permanent dipole interaction. A potential energy surface was generated by modulating the three contributions, ensuring the continuity of the analytical potential energy surface and producing a maximum effect at the Ne*−C−Cl angle of 45°. It is obvious that the electrostatic term plays an important role since the potential energy surface was drastically changed upon inclusion of the electrostatic term. It is expected that the difference between the interaction potentials for the Li−C_2H_5Cl and Li−C_2H_5F systems, as obtained by the present ab initio MO calculations, cannot be reproduced semiempirically, because the angular distributions of the potential energy in the electrostatic term for both systems are expected to be nearly equivalent.

Serious problems of the semiempirical potential model are summarized as follows. (i) In molecular systems, interactions are highly anisotropic. (ii) It is very difficult to unambiguously determine the three contributions in the model. (iii) Quantum chemical interactions between molecular orbitals are not necessarily describable by simple electrostatic interactions of local electric moments. To avoid such difficulties, quantum chemical ab initio MO methods are preferable if ab initio MO computations are tractable.

Experimental results found in the present work show good agreement with the results of ab initio MO calculation, indicating that potential energy surfaces calculated by ab initio MO method are more reliable than those obtained by semiempirical procedure outlined above.

VI. Conclusion

In this study, the results of PIES of C_2H_5Cl and C_2H_5F due to metastable He*(2^3S) atoms were presented. Specific incident approach angle dependence of reactivity around Cl atom is obtained. The He* atom approach coming from the opposite side of the CH_3 group toward the perpendicular to the C−Cl axis gives the most attractive interaction. On the other hand, the most attractive interaction is distributed over the C−F axis direction in the He*−C_2H_5F system. In this case, the attractive interaction centered at C−F bond axis shows wide and deep potential well. This wide attractive region around the F atom governs the reactivity of the C_2H_5F molecule. It is noted that anisotropic interactions around the F and Cl atoms with He* atom in C_2H_5X (X = Cl, F) are well correlated to those around the O and S atoms with He* atom in C=X (X = O, S) group. Namely, the attractive interaction was dominated around the direction collinear with the bond axis for the first row elements (O, F), while for the second row elements (S, Cl) the attractive interaction was localized around the direction perpendicular to the bond axis. These differences owing to the periodicity may be ascribed to the presence of different types of orbital interactions between the C atom and first row elements and to the second row elements, respectively. The similar ionization potentials for second row elements and the C atom imply that the p-orbital character of the second row atoms along the bond axis diminishes due to the bond formation with the C atom because the contribution of each atomic p orbitals for the bond formation is almost equivalent. On the other hand, the p orbital contribution of the first row atoms is larger, since their ionization potentials are higher than that of the C atom. As a consequence, the p-orbital character along the bond axis becomes important for the Penning ionization reaction.

Acknowledgment. This work has been partially supported by a Grant in Aid for Scientific Research from the Japanese Ministry of Education, Science, and Culture. One of the authors (K.I) thanks the Japan Society for the Promotion of Science (JSPS) for a JSPS Research Fellowship.

References and Notes

(1) Ohno, K.; Mutoh, H.; Harada, Y. *J. Am. Chem. Soc.* **1983**, *105*, 4555.

(2) Ohno, K.; Harada, Y. *Molecular Spectroscopy, Electronic Structure and Intramolecular Interactions*; Maksić, Z. B., Ed.; Springer-Verlag: Berlin Heidelberg, 1991; p 199.

(3) Penning, F. M. *Naturwissenschaften* **1927**, *15*, 818.

(4) Hotop, H.; Niehaus, A. *Z. Phys.* **1969**, *228*, 68.

(5) Ohno, K.; Matsumoto, S.; Harada, Y. *J. Chem. Phys*. **1984**, *81*, 4447.

(6) Siska, P. E. *Rev. Mod. Phys*. **1993**, *65*, 337, and references therein.

(7) Yamakado, H.; Yamaguchi, M.; Hoshino, S.; Ohno, K. *J. Phys. Chem*. **1995**, *99*, 55.

(8) Ohno, K.; Yamakado, H.; Ogawa, T.; Yamata, T. *J. Chem. Phys*. **1996**, *105*, 7536.

(9) Ohno, K.; Kishimoto, N.; Yamakado, H. *J. Phys. Chem.* **1995**, *99*, 9687.

(10) Yamakado, H.; Okamura, K.; Ohshimo, K.; Kishimoto, N.; Ohno, K. *Chem. Lett*. **1997**, 269.

(11) Kishimoto, N.; Ohshimo, K.; Ohno, K. *J. Electron Spectrosc. Relat. Phenom*. **1999**, *104*, 145.

(12) Takami, T.; Mitsuke, K.; Ohno, K. *J. Chem. Phys*. **1991**, *95*, 918.

(13) Tokue, I.; Sakai, Y.; Yamasaki, K. *J. Chem. Phys*. **1997**, *106*, 4491.

(14) Alberti, M.; Lucas, J. M.; Brunetti, B.; Pirani, F.; Stramaccia, M.; Rosi, M.; Vecchiocattivi, F. *J. Phys. Chem. A* **2000**, *104*, 1405.

(15) Yamato, M.; Okada, S.; Wu, V. W.-K.; Ohoyama, H.; Kasai, T. *J. Chem. Phys*. **2000**, *113*, 6673.

(16) (a) González, M.; Sierra, J. D.; Francia, R.; Sayós, R. *J. Phys. Chem. A* **1997**, *101*, 7513. (b) Gericke, K. H.; Kreher, C.; Rinnenthal, J. L. *J. Phys. Chem. A* **1997**, *101*, 7530. (c) Meijer, A. J. H. M.; Groenenboom, G. C.; van der Avoird, Ad. *J. Phys. Chem. A* **1997**, *101*, 7558. (d) Grosser, J.; Hoffmann, O.; Rakete, C. *J. Phys. Chem. A* **1997**, *101*, 7627. (e) Aquilanti, V.; Ascenzi, D.; Cappelletti, C.; Fedeli, R.; Pirani, F. *J. Phys. Chem. A* **1997**, *101*, 7648.

(17) Loesch, H. J. *Annu. Rev. Phys. Chem.* **1995**, *46*, 555.

(18) (a) Loesch H. J.; Stienkemeier, F. *J. Chem. Phys*. **1993**, *98*, 9570. (b) Loesch, H. J.; Stienkemeier, F. *J. Chem. Phys*. **1994**, *100*, 740. (c) Loesch, H. J.; Stienkemeier, F. *J. Chem. Phys*. **1994**, *100*, 4308.

(19) Kishimoto, N.; Osada, Y.; Ohno, K. *J. Phys. Chem. A* **2000**, *104*, 1393.

(20) Mitsuke, K.; Takami, T.; Ohno, K. *J. Chem. Phys*. **1989**, *91*, 1618.

(21) Ohno, K.; Takami, T.; Mitsuke, K.; Ishida, T. *J. Chem. Phys*. **1991**, *94*, 2675.

(22) Takami, T.; Ohno, K. *J. Chem. Phys*. **1992**, *96*, 6523.

(23) Gardner, J. L.; Samson, J. A. R. *J. Electron Spectrosc. Relat. Phenom*. **1976**, *8*, 469.

(24) Kimura, K.; Katsumata, S.; Achiba, Y.; Yamazaki, T.; Iwata, S. *Handbook of He I Photoelectron Spectra of Fundamental Organic Molecules*; Japan Scientific: Tokyo, 1981.

(25) Turner, D. W.; Baker, C.; Baker, A. D.; Brundle, C. R. *Molecular Photoelectron Spectroscopy*; Wiley: London, 1970.

(26) Yee, D. S. C.; Stewart, W. B.; Mcdowell, C. A.; Brion, C. E. *J. Electron Spectrosc. Relat. Phenom*. **1975**, *7*, 93.

(27) Hotop, H.; Hubler, G. *J. Electron Spectrosc. Relat. Phenom*. **1977**, *11*, 101.

(28) Auerbach, D. J. *Atomic and Molecular Beam Methods*; Scoles, G., Ed.; Oxford University: New York, 1988; p 369.

(29) Hirota, M.; Iijima, T.; Kimura, M. *Bull. Chem. Soc. Jpn*. **1978**, *51*, 1594.

(30) Zeil, W.; Christen, D. *J. Phys. Chem*. **1980**, *84*, 1790.

(31) Beagley, B.; Jones, M. O.; Yavari, P. *J. Mol. Struct*. **1981**, *71*, 203.

(32) Pauling, L. *The Nature of the Chemical Bond*; Cornell University: Ithaca, New York, 1960.

(33) Rothe, E. W.; Neynaber, R. H.; Trujillo, S. M. *J. Chem. Phys*. **1965**, *42*, 3310.

(34) Illenberger, E.; Niehaus, A. *Z. Phys. B* **1975**, *20*, 33.

(35) Parr, T.; Parr, D. M.; Martin, R. M. *J. Chem. Phys*. **1982**, *76*, 316.

(36) Hotop, H. *Radiat. Res*. **1974**, *59*, 379.

(37) Haberland, H.; Lee, Y. T.; Siska, P. E. *Adv. Chem. Phys*. **1981**, *45*, 487.

(38) Hotop, H.; Roth, T. E.; Ruf, M.-W.; Yencha, A. J. *Theor. Chem. Acc*. **1998**, *100*, 36.

(39) Frisch, M. J.; Trucks, G. W.; Schlegel, H. B.; Gill, P. M. W.; Johnson, B. G.; Robb, M. A.; Cheeseman, J. R.; Keith, T.; Petersson, G. A.; Montgomery, J. A.; Raghavachari, K.; Al-Laham, M. A.; Zakrzewski, V. G.; Ortiz, J. V.; Foresman, J. B.; Cioslowski, J.; Stefanov, B. B.; Nanayakkara, A.; Challacombe, M.; Peng, C. Y.; Ayala, P. Y.; Chen, W.; Wong, M. W.; Andres, J. L.; Replogle, E. S.; Gomperts, R.; Martin, R. L.; Fox, D. J.; Binkley, J. S.; Defrees, D. J.; Baker, J.; Stewart, J. P.; Head-Gordon, M.; Gonzalez, C.; Pople, J. A. *Gaussian 94*, revision D.4 Gaussian, Inc.: Pittsburgh, PA, 1995.

(40) von Niessen, W.; Schirmer, J.; Cederbaum, L. S. *Comput. Phys. Rep*. **1984**, *1*, 57.

(41) (a) Zakrzewski, V. G.; Ortiz, J. V. *Int. J. Quantum Chem. Symp*. **1994**, *28*, 23. (b) Zakrzewski, V. G.; Ortiz, J. V. *Int. J. Quantum Chem.* **1995**, *53*, 583.

(42) Katsumata, S.; Kimura, K. *J. Electron Spectrosc. Relat. Phenom*. **1975**, *6*, 309.

(43) Katsumata, S.; Iwai, T.; Kimura, K. *Bull. Chem. Soc. Jpn*. **1973**, *46*, 3391.

(44) Ortiz, J. V.; Zakrzewski, V. G.; Dolgounitcheva, O. *Conceptual Perspectives in Quantum Chemistry*; Calais, J.-L., Kryachko, E., Eds.; Kluwer Academic Publishers: Dordrecht, 1997; p 465.

(45) Ohno, K.; Imai, K.; Matsumoto, S.; Harada, Y. *J. Phys. Chem*. **1983**, *87*, 4346.

(46) Handy, N. C.; Marron, M.; Silverstone, H. *J. Phys. Rev*. **1969**, *180*, 45.

(47) Ahlrichs, R. *Chem. Phys. Lett*. **1973**, *18*, 521.

(48) Morrell, M. M.; Parr, R. G.; Levy, M. *J. Chem. Phys*. **1975**, *62*, 549.

(49) Katriel, J.; Davidson, E. R. *Proc. Natl. Acad. Sci*. U.S.A, **1980**, *77*, 4403.

(50) Yamazaki, T.; Kimura, K. *Bull. Chem. Soc. Jpn*. **1975**, *48*, 1602.

(51) Brunetti, B.; Candori, P.; De Andres, J.; Pirani, F.; Rosi, M.; Falcinelli, S.; Vecchiocattivi, F. *J. Phys. Chem. A* **1997**, *101*, 7505, and references therein.